Letters

Multiresonant-Frequency Filter for an Electrosurgery Inverter

Congbo Bao, *Graduate Student Member, IEEE*, and Sudip K. Mazumder, *Fellow, IEEE*

***Abstract*—This letter presents a multiresonant-frequency (MRF) filter for a high-frequency inverter (HFI) used in electrosurgery. The fundamental (sinusoidal) output frequency of the HFI is 390 kHz and is the same as the switching frequency of the HFI. The MRF is designed to extract the fundamental frequency of the tri-state bipolar waveform, generated by the HFI operating with phase-shift control. The structure and operation of the MRF are outlined. An experimental 300-W GaN-FET-based HFI prototype is developed to validate the feasibility of the proposed MRF under closed-loop control.**

***Index Terms*—Control, electrosurgery, GaN, high-frequency inverter, multiresonant-frequency filter.**

I. Introduction

MORTON, in 1881, showed that a human being's muscle stimulation terminates whenever the applied signal frequency is higher than 100 kHz [1]. Based on that, electrosurgery was first invented in 1926 by William Bovie [1] and the illustration of the monopolar surgery using the electrosurgery generator is demonstrated in Fig. 1. Modern electrosurgery passes alternating signals with a fundamental frequency above 200 kHz but lower than 5 MHz through the human body to conduct clinical treatment, such as cutting, coagulation, and fulguration, etc. [2], [3]. Therefore, inverters with HF outputs are required for electrosurgery.

Resonant inverters (e.g., class E, F, EF_2, Class Φ_2) and their variants feature HF output with reasonable efficiency [4]. However, none of those topologies has been investigated in the area of electrosurgery due to certain limitations, such as load sensitivity, high device voltage stress, and sophisticated tuning processes [5]. Wide-bandgap (e.g., SiC, GaN) device-based PWM inverters can operate at HF. However, to generate a fundamental (inverter-sinusoidal-output) frequency of at least 200 kHz, as needed by electrosurgery, an extremely high switching frequency (multi-MHz) is needed that is impractical from efficiency, thermal, and electromagnetic interference standpoints.

Manuscript received October 9, 2021; revised November 29, 2021; accepted December 19, 2021. This work was supported by the National Institute of Biomedical Imaging and Bioengineering of the National Institutes of Health under Award R01EB029766. *(Corresponding author: Sudip K. Mazumder.)*

The authors are with the Electrical and Computer Engineering Department, University of Illinois at Chicago, Chicago, IL 60607 USA (e-mail: cbao5@uic.edu; mazumder@uic.edu).

Color versions of one or more figures in this article are available at https://doi.org/10.1109/TPEL.2021.3137525.

Digital Object Identifier 10.1109/TPEL.2021.3137525

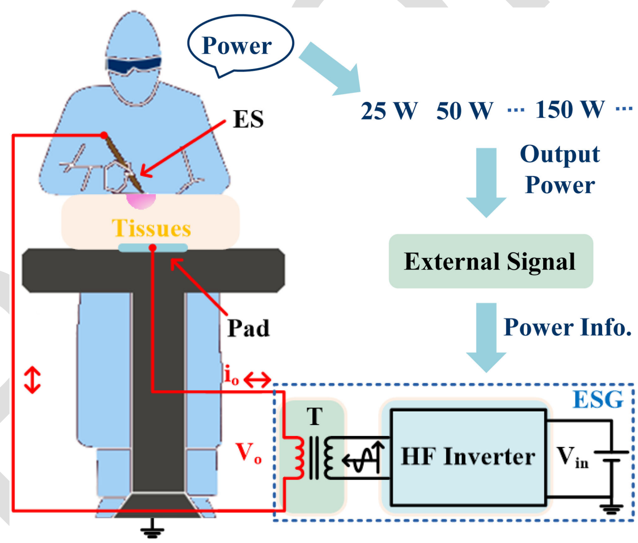

Fig. 1. Demonstration of monopolar surgery using an electrosurgery generator. The HF step-up transformer for galvanic isolation is abbreviated as T and the electric scalpel is noted as ES. The biomedical tissues are placed between the ES and the return pad to close the path for current flow. The surgeon selects the modes according to his/her electrosurgery needs.

Selective harmonic elimination (SHE) was pursued in line-frequency-commutated converters decades back owing to very-slow thyristor and triac. However, the introduction of notches is still required for extracting the fundamental-frequency output at an acceptable THD and hence application of SHE will still require an electrosurgery HF inverter to operate at frequencies that are multiples of 200 kHz yielding similar challenges abovementioned.

The existing literature on inverters for electrosurgery (e.g., [6], [7], etc.) either outline inverters that generate square-wave output with a much higher switching frequency that yields higher switching loss and more importantly potentially tissue-damaging super-harmonics or soft-switched inverters that reduce the switching loss but can only support very narrow load range (to achieve soft switching) and further, the load range bounds are also well short of the ones needed for supporting electrosurgery [1], [2].

For this reason, the multiresonant-frequency (MRF) is proposed to tackle the HF inverter challenges faced in the electrosurgery area. This letter introduces the MRF structure, HF generation mechanism, and its actual inductance-based transfer

0885-8993 © 2021 IEEE. Personal use is permitted, but republication/redistribution requires IEEE permission.
See https://www.ieee.org/publications/rights/index.html for more information.

IEEE Proof

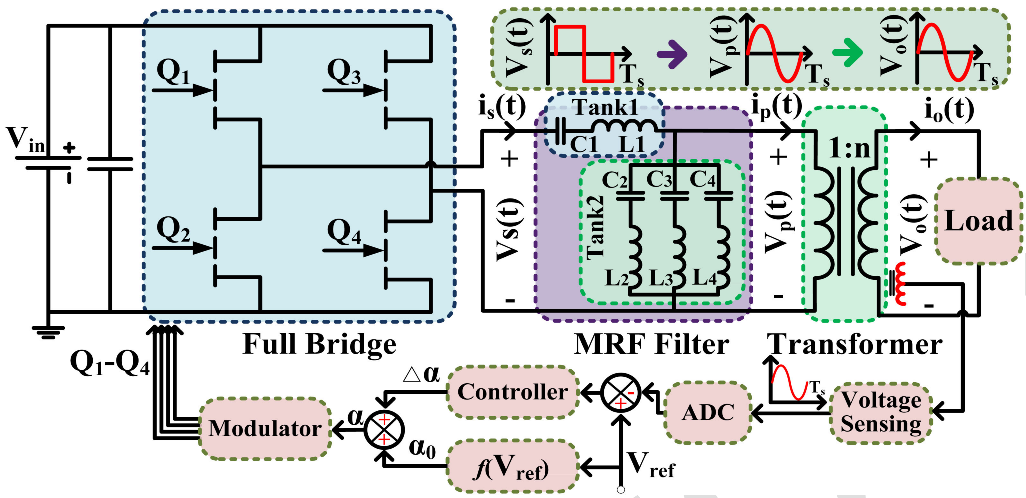

Fig. 2. Topology of the full-bridge- and MRF-based HFI. The HFI employs phase-shift control to generate a bipolar square waveform which is shaped into a sinusoidal (fundamental) waveform by the MRF filter. Transformer turn ratio is designated as n and its secondary side is directly connected to the load. The output voltage regulation is achieved via adjustment of full-bridge phase-shift angle α, which is derived from the angular information of the feedforward output signal α_0 and the controller output signal $\Delta\alpha$.

function. Based on that, experimental results showing closed-loop performances are provided to justify the feasibility of the proposed MRF.

II. HF Output Generation and MRF

A. HF Output Generation Mechanism

The proposed high-frequency inverter (HFI) topology together with its closed-loop control diagram is shown in Fig. 2. Dc input of the HFI is denoted by V_{in} and GaN FETs, switching at 390 kHz under phase shift, which are represented by $Q_{1\text{-}4}$. When diagonal devices Q_1 and Q_4 (or Q_2 and Q_3) are turned ON at the same time, full-bridge output equals V_{in} (or -V_{in}), otherwise, the output is zero. The ideal output of the HFI, $V_s(t)$, is delineated as a bipolar square waveform of 390 kHz, which is expressed using a Fourier series as follows [8]:

$$V_s\left(t\right) = \frac{4\mathrm{V}_{\text{in}}}{\pi} \cdot \frac{1}{n} \cdot \cos\left(\alpha\right) \cdot \Sigma_{n=1,3,5,\ldots\infty}^{\infty} \sin\left(2\pi n f_s t\right) \quad (1)$$

where n and α are the order of the harmonics and the phase shift angle, respectively. The MRF practically suppresses the odd harmonics in $V_s(t)$ and only the fundamental frequency component of $V_s(t)$, appears in the transformer primary side and delivers energy to load via the high-frequency step-up transformer. Consequently, the output frequency of the HFI is the same as the switching frequency of the GaN-based HFI.

B. MRF

The proposed MRF, as shown in Fig. 2, consists of two resonant tanks. Resonant tank-1 is tuned to resonate at 390 kHz while tank-2 resonates at third, fifth, and seventh order harmonics. An infinite number of resonant branches in tank-2 is theoretically required to eliminate all odd frequencies in $V_s(t)$, as shown in (1). However, it turns out three resonant branches in tank-2 are good enough to achieve satisfied THD in practice without the need for ninth or higher resonant branches. Owing to this special structure and combination, the MRF represents different impedances to the fundamental and higher order harmonic components, which is illustrated in Fig. 3(a) and (d). Tank-1 resonates at 390 kHz, and thus, presents zero impedance at f_s, as manifested in Fig. 3(a). As shown in Fig. 3(b) and (d), tank-2 yields zero impedances for the third, fifth, and seventh harmonics.

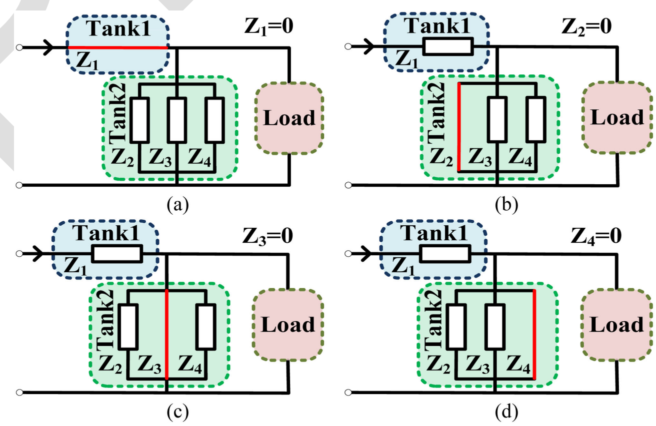

Fig. 3. Tank impedance for different frequencies and the short path is marked in red. (a) Fundamental frequency (390 kHz). (b) Third harmonic. (c) Fifth harmonic. (d) Seventh harmonic.

For the MRF, tank-1 L_1 is based on CoilCraft AGP4233 series inductor. For tank-2, SER2211 and SER1390 series inductors from CoilCraft are used for L_2–L_4. Finally, all resonant

IEEE Proof

IEEE Proof

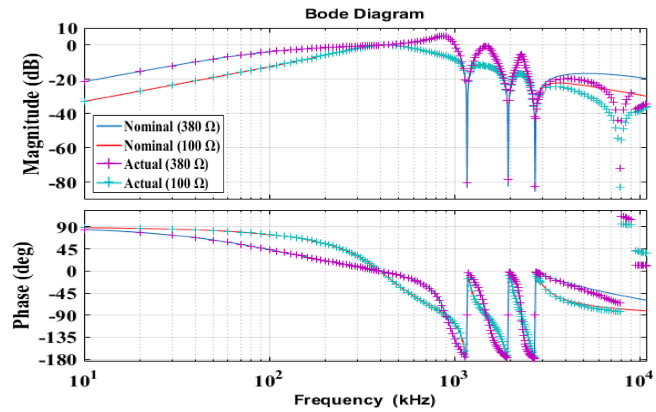

Fig. 4. Actual- and nominal-inductance based Bode plots of the MRF when it is directly connected to a 100 Ω (or 380 Ω) load (which is equivalent to a 570 Ω (or 2.2 kΩ) load as seen from the secondary side if a transformer with a 2.396 turn ratio is connected).

capacitors are based on C0G dielectric. The MRF transfer function for a given load (*R*) is determined to be the following:

$$TF_{\mathrm{MRF}}\ (s) = \frac{V_p\,(t)}{V_s\,(t)} = \frac{Z_{\mathrm{tank2}}\,(s)\,||R}{\{Z_{\mathrm{tank2}}\,(s)\,||R)\} + Z_{\mathrm{tank1}}\,(s)} \tag{2}$$

where

$$Z_{\mathrm{tank1}}\ (s) = s \cdot L_1 + \frac{1}{sC_1}$$

$$Z_{\mathrm{tank2}}\ (s) = \frac{1}{\frac{1}{s\cdot L_2 + {}^1/_s \cdot C_2} + \frac{1}{s\cdot L_3 + {}^1/_s \cdot C_3} + \frac{1}{s\cdot L_4 + {}^1/_s \cdot C_4}}$$

and is plotted in Fig. 4. The nominal plot shown in Fig. 4 represents (2) based on the nominal tank parameters. The other plot is based on actual (practical) tank parameters and shows some modest deviation primarily at high frequency (i.e., beyond the fundamental). This deviation is mainly attributed to L_1, which attains progressively higher values with increasing excitation frequency toward the self-resonant frequency of L_1. Tank-2 *LC* parameters are more stable over the frequency range considered in this letter. Overall, and as shown in Fig. 4, the two Bode plots both yield 0 dB at 390 kHz and possess small gain at both high-order harmonics (e.g., third, fifth, and seventh, etc.) and frequencies lower than 100 kHz, which distinguishes the MRF from conventional low-pass filters, such as *LCL*, and *LLCL*, etc. [9]. Because of such gain characterization, an output of low THD and suppression of frequencies causing muscle stimulation are achieved, simultaneously [1]. However, two Bode plots differ from each other when the frequency exceeds multi-MHz and the actual inductance-based Bode plot imposes higher attenuation. Given the special Bode plot property of the MRF, frequency spectrum components contained in $V_s(t)$ are treated differently, as shown in Fig. 5. It is apparent that, the fundamental component of the HFI is passed to the load without reduction whereas other higher harmonics are blocked. Consequently, the bipolar square waveform is shaped into a sinusoidal output, and the transformer primary side voltage,

TABLE I
EXPERIMENT PARAMETERS USED IN THIS LETTER

Parameters	Values
Capacitor C_1~ C_4	3543 *p*F, 196 *p*F, 141 *p*F, 154 *p*F
Inductor L_1~ L_4	47 µH, 94 µH, 47 µH, 22 µH
Switching frequency f_s	390 kHz
Transformer turn ratio	2.396
PI parameters	$K_p = 4.0$, $K_i = 8.0$
Load resistor	LPS 600 series

$V_p(t)$, is determined as follows:

$$V_p\ (t) = \frac{4V_{\mathrm{in}}}{\pi} \cdot \cos(\alpha) \cdot \sin(2\pi f_s t)\,. \tag{3}$$

III. Experimental Results

A 300-W GaN-based HFI hardware prototype, as shown in Fig. 6, is designed, fabricated, and tested to validate the proposed MRF. The PWM signal is generated by a TMS320F28379D dual-core DSP controller and the GaN devices are GS66508B from GaN System. The detailed hardware parameters are tabulated and listed in Table I.

A. Output Regulation and THD

As indicated by (3), the phase shift angle α regulates the transformer's primary side voltage, and thus, secondary-side voltage, V_o(t). The theoretical output voltage and experimental measurements are compared and plotted in Fig. 7 when the dc input is set as 50, 100, and 150 V. The comparison result indicates that the hardware measurements match the theoretical calculation with minimal errors and justify the controllability of α on V_o(t). The output voltage THD for closed-loop control is plotted in Fig. 8 versus different output powers and various output load resistances. It is noted that output voltage THD is quite small and the maximum THD for HFI is 3.28% and 4.23% in Fig. 8(a) and (b), respectively. Furthermore, output THD remains small, as shown in Fig. 9, even when the tank-1 capacitor deviates from its nominal value. It is worth mentioning that output voltage regulation errors slightly deteriorate as the deviation and load resistance increase.

B. Closed-Loop Transient Results

To showcase the controllability of the proposed MRF, the closed-loop control diagram for output voltage regulation is given in Fig. 2. The combination of feedforward and proportional–integral (PI) control strategy is employed. The PI parameters are listed in Table I and the feedforward function to calculate α_0 is noted as follows:

$$\alpha_0 = f(V_{\mathrm{ref}}) = \frac{180}{\pi} \cdot \cos^{-1}\left(\frac{\pi \cdot V_{\mathrm{ref}}}{4 \cdot \mathrm{n} \cdot V_{\mathrm{in}}}\right). \tag{4}$$

The feedforward block provides an initial phase shift angle α_0 and the PI controller output $\Delta\alpha$ compensates for the remaining regulation errors by adjusting the phase shift angle α between gate signals of diagonal switch pairs (Q_1 and Q_4 or Q_2 and Q_3).

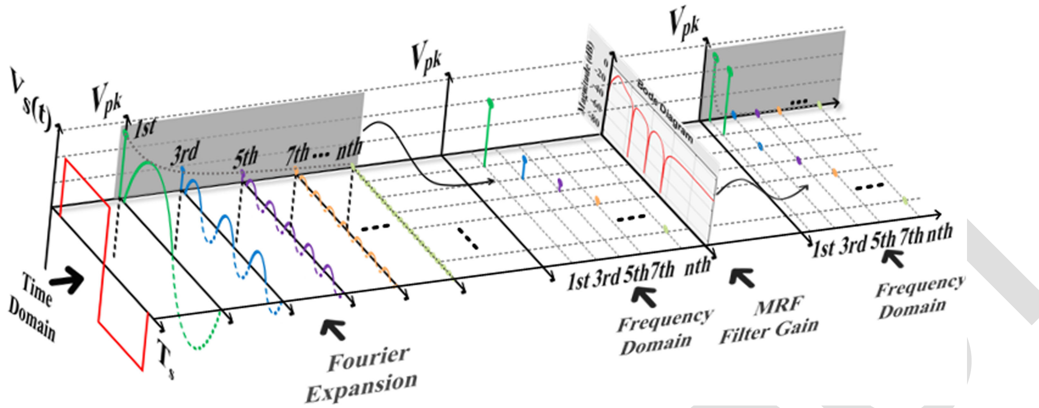

Fig. 5. Frequency spectrum of the HFI bipolar square waveform and the corresponding MRF attenuation.

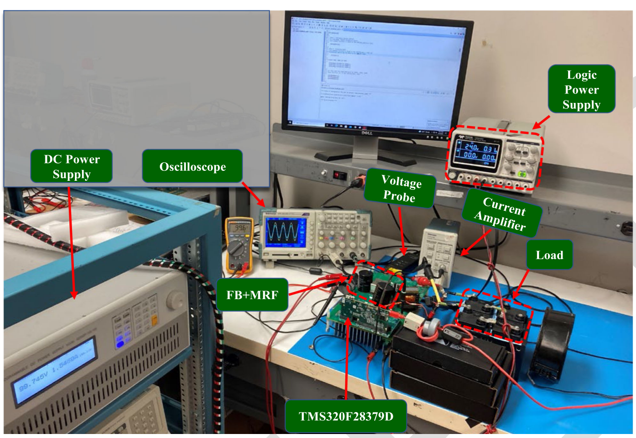

Fig. 6. Experimental setup of the HFI.

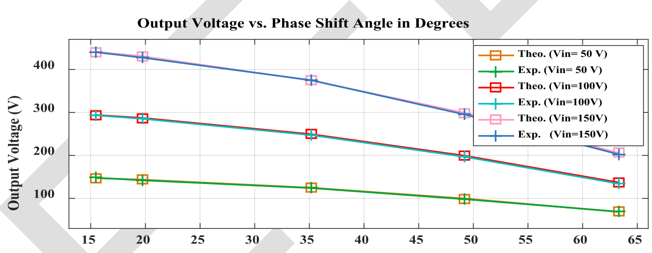

Fig. 7. Output voltage versus phase shift angle for three different dc inputs.

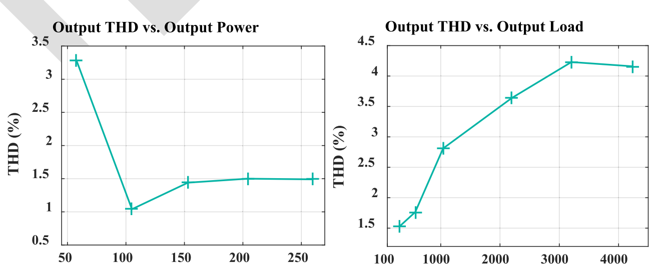

(a) (b)

Fig. 8. Output THD for the HFI. (a) Output powers that are adjusted by varying phase shift α and V_{in} is set as 100 V. (b) Output load resistances ranging from 300 to 4200 Ω. V_{in} is set as 100 V (200 V) for load resistances lower (higher) than 1 kΩ.

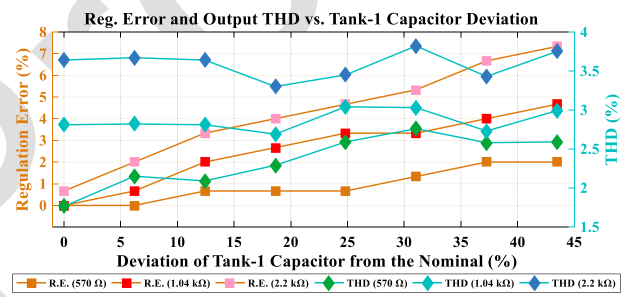

Fig. 9. Output voltage regulation errors (R.E.) and THD at the different load resistances versus tank-1 capacitor deviating from its nominal value.

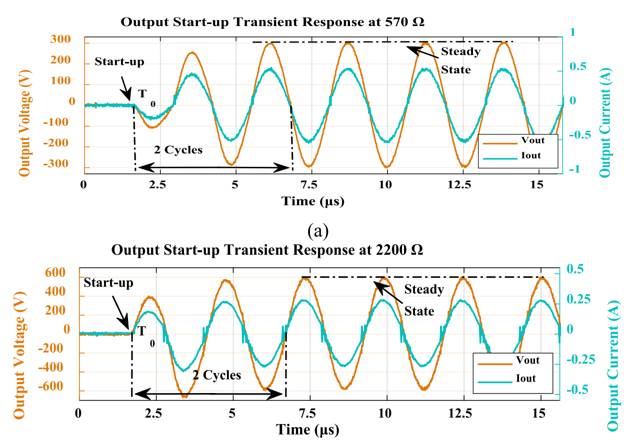

(b)

Fig. 10. Output start-up transient response of the HFI. Trace with higher magnitude represents the output voltage. (a) For a load resistance of 570 Ω with V_{in} and V_{ref} set at 100 V and 300 V, respectively, and (b) for a load resistance of 2.2 kΩ with V_{in} and V_{ref} set at 200 V and 600 V, respectively.

Based on the control diagram, output start-up transient from zero-state to steady state is plotted in Fig. 10. The HFI starts at T_0 and reaches the V_{ref} in two switching cycles. Furthermore, output dynamics are provided in Fig. 11 for a step-change in the load. The output voltage slightly reduces at T_1 and then quickly returns to steady state in three cycles. The output has a small overshoot at T_2 and then settles to steady state in three switching cycles.

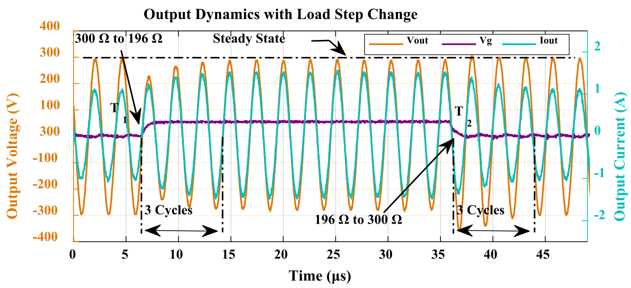

(a)

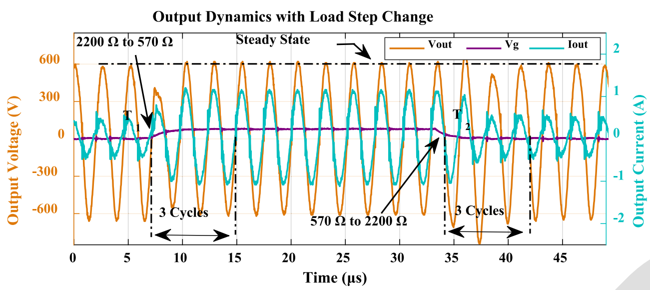

(b)

Fig. 11. Output-voltage dynamics for a step change in the load. The load comprises a 300 Ω (2200 Ω) load resistor in parallel with a switched 570 Ω (770 Ω) load resistor. So by default, the load is 300 Ω (2200 Ω) and when the switch is turned ON, the load changes to 196 Ω (570 Ω). The purple trace (V_g) is the gate signal of the switch triggering the load step change with 15 V. (a) Step change in the load from 300 to 196 Ω at T_1 and 196 to 300 Ω at T_2, respectively, with V_{in} as 100 V. (b) Step change in the load from 2200 to 570 Ω at T_1 and 570 to 2200 Ω at T_2, respectively, with V_{in} as 200 V. Output current for a load of 2200 Ω is modestly distorted due to loading effect of the switch parasitics and the normal steady-state current is shown in Fig. 10. Among the two sinusoidal type traces, trace with higher magnitude represents the output voltage.

IV. Conclusion

This letter outlines an MRF of a full-bridge-based HFI for electrosurgery. It enables the fundamental output and switching frequency of the HFI to be the same at 390 kHz without requiring complex, or very-high-frequency PWM or expensive solutions. The HF output generation mechanism is explained and the MRF structure and its transfer function are provided as well. A 300 W experimental GaN-based HFI is developed and tested. The experiment results show that the HFI has the capability of regulating output voltage via phase-shift angle. Meanwhile, the HFI also supports a wide range of loads with low output voltage THD under various output powers and load conditions. Furthermore, output THD and regulation errors remain small as the tank-1 capacitor deviates from its nominal value. However, the output THD and current quality slightly deteriorate at light load and high load resistance, which can be improved by properly optimizing the transformer turn ratio. Finally, the feedforward and PI-based control ensures that the transient performance of the HFI is found to be satisfactory despite high order of the HFI, as validated using transient and load step changes experimental results.

Acknowledgment

The content is solely the responsibility of the authors and does not necessarily represent the official views of the National Institutes of Health. The authors would like to thank S. Gupta, a doctoral student in the Laboratory for Energy and Switching-Electronic Systems of the University of Illinois Chicago, for his help with DSP coding. They also express their thanks to Prof. J. Bentsman, who serves as the lead PI at the University of Illinois Urbana-Champaign.

References

[1] N. N. Massarweh, N. Cosgriff, and D. P. Slakey, "Electrosurgery: History, principles, and current and future uses," *J. Amer. College Surgeons*, vol. 202, no. 3. pp. 520–530, Mar. 2006.

[2] "User's guide force FX^{TM}-C electrosurgical generator with instant response^{TM} technology," 2009, Accessed: Nov. 24, 2020. [Online]. Available: https://www.equippedmd.com/wp-content/uploads/2018/01/Valleylab-Force-FX-C-Operators-Guide.pdf

[3] International Electrotechnical Commission (IEC), "Medical electrical equipment - Part 2-2: Particular requirements for the basic safety and essential performance of high frequency surgical equipment and high frequency surgical accessories," 2017, Accessed: Aug. 24, 2021. [Online]. Available: https://webstore.iec.ch/publication/28118

[4] J. M. Rivas, Y. Han, O. Leitermann, A. D. Sagneri, and D. J. Perreault, "A high-frequency resonant inverter topology with low-voltage stress," *IEEE Trans. Power Electron.*, vol. 23, no. 4, pp. 1759–1771, Jul. 2008.

[5] C. Bao and S. K. Mazumder, "GaN-HEMT based very-high-frequency ac power supply for electrosurgery," in *Proc. IEEE Appl. Power Electron. Conf. Expo.*, Jul. 2021,pp. 220–225.

[6] S. Jensen and D. Maksimovic, "Fast tracking electrosurgical generator using two-rail multiphase buck converter with GaN switches," *IEEE Trans. Power Electron.*, vol. 32, no. 1, pp. 634–641, Jan. 2017.

[7] S. Jensen, L. Corradini, M. Rodriguez, and D. Maksimovic, "Modeling and digital control of LCLC resonant inverter with varying load," in *Proc. IEEE Energy Convers. Congr. Expo. Energy Convers. Innov. Clean Energy Future*, 2011, pp. 3823–3829.

[8] R. W. Erickson and D. Maksimović, *Fundamentals of Power Electronics*. Berlin, Germany: Springer, 2020.

[9] W. Wu, Y. He, and F. Blaabjerg, "An LLCL power filter for single-phase grid-tied inverter," *IEEE Trans. Power Electron.*, vol. 27, no. 2, pp. 782–789, Jul. 2012.

IEEE Proof